JOURNAL OF GEOPHYSICAL RESEARCH: ATMOSPHERES, VOL. 118, 12,359–12,370, doi:10.1002/2013JD019914, 2013

Northern Hemispheric cryosphere response to volcanic eruptions in the Paleoclimate Modeling Intercomparison Project 3 last millennium simulations

Mira Berdahl[1] and Alan Robock[1]

Received 27 March 2013; revised 28 October 2013; accepted 29 October 2013; published 20 November 2013.

[1] We analyzed last millennium simulations (circa 850–1850 Common Era) from the Paleoclimate Modeling Intercomparison Project 3 (PMIP3) project to determine whether current state-of-the-art models produce sudden changes and persistence of cold conditions after large volcanic eruptions as inferred from geological records and previous climate modeling. Snow cover over Baffin Island in the eastern Canadian Arctic shows large-scale expansion (as seen in proxy records) in two of the five models with snow cover information available, although it is not sustained beyond a decade. Sea ice expansion in the North Atlantic is seen in some PMIP3 models after large eruptions, although none of these models produce significant centennial-scale effects. Warm Baffin Island summer climates stunt snow expansion in some models completely, and model topography tends to miss the critical plateau elevations that could sustain snow on the island. Northern Hemisphere sea ice extent is lower in six of the eight models than in reconstructions over the past millennium. Annual average Northern Hemisphere mean climates have a range of 3 K across models, while Arctic summer land-only climates span more than 6 K. This has critical consequences on ice and snow formation and persistence in regions such as the Arctic where temperatures are near the freezing point and small temperature changes affect ice and snow feedback that could induce further climate changes. Thus, it is critical that models accurately represent absolute temperature.

Citation: Berdahl, M., and A. Robock (2013), Northern Hemispheric cryosphere response to volcanic eruptions in the Paleoclimate Modeling Intercomparison Project 3 last millennium simulations, *J. Geophys. Res. Atmos.*, *118*, 12,359–12,370, doi:10.1002/2013JD019914.

1. Introduction

[2] Earth's temperature history over the past millennium provides a critical framework for accurately generating and understanding projections of future change. Northern Hemisphere (NH) proxy reconstructions over this period [*Mann et al.*, 2009, 2008; *Jansen et al.*, 2007] have large uncertainties and show variable timing, amplitude, and spatial extent of multidecadal events such as the Little Ice Age (LIA, circa 1300–1850 Common Era (C.E.)) and the Medieval Climate Anomaly (circa 900–1250 C.E.) [*Frank et al.*, 2010; *Miller et al.*, 2010]. Climate models are one of the most valuable tools used in the study of the last millennium, since they can help unravel the fundamental underlying mechanisms controlling the climate system.

[3] Volcanism is the most prominent natural forcing factor for climate variability of the last 700 years [*Hegerl et al.*, 2007]. It is well known that strong volcanic eruptions (SVEs) can have a major impact on the global climate through radiation impacts on the atmosphere [*Robock*, 2000], which in turn impact ocean dynamics [e.g., *Mignot et al.*, 2011; *Miller et al.*, 2012]. SVEs tend to cool the global climate for several years and can also cause regional effects such as monsoon disruptions and winter warming over the NH continents [*Robock*, 2000].

[4] *Miller et al.* [2012] presented data from ice caps on the plateaus of Baffin Island in the eastern Canadian Arctic, showing intermittent ice melt and growth between the late thirteenth century and the mid-fifteenth century, followed by continuous ice cover from the mid-fifteenth century until roughly a century ago. The sudden cooling in the mid-thirteenth century coincides with four roughly decadally paced eruptions, the first of which is the 1257 Samalas eruption [*Lavigne et al.*, 2013], the largest eruption in the last 7000 years [*Langway et al.*, 1988]. The snow expansion affected sites in north-central Baffin Island in the elevation range of 660–1000 m [*Miller et al.*, 2012], dropping into the shallowly undulating plateaus of 400–700 m [*Andrews et al.*, 1972]. Lowering the snowline into this region could cause a drastic increase in snow coverage. *Berdahl and Robock* [2013] found that in a 10 km resolution regional climate model, a summer temperature decrease of 3.9 ± 1.1 K from the current climate was necessary to lower the snowline by comparable elevation changes seen during the descent into the LIA on Baffin Island.

[5] Proxy records and some modeling experiments [*Briffa et al.*, 1998; *Zhong et al.*, 2010; *Miller et al.*, 2012; *Schleussner*

[1]Department of Environmental Sciences, Rutgers University, New Brunswick, New Jersey, USA.

Corresponding author: M. Berdahl, Department of Environmental Sciences, Rutgers University, 14 College Farm Rd., New Brunswick, NJ 08901, USA. (mberdahl@envsci.rutgers.edu)

2169-897X/13/10.1002/2013JD019914

Table 1. Last Millennium Simulations Modeling Groups and Model Acronyms and Volcanic and Solar Forcing, Adapted From *Brohan et al.* [2012]

Acronym	Modeling Group	Volcanic/Solar Forcing
BCC	Beijing Climate Center, China Meteorological Administration [*Wu et al.*, 2013]	*Gao et al.* [2008]/*Vieira and Solanki* [2010]
GISSG	NASA Goddard Institute for Space Studies [*Schmidt et al.*, 2006]	*Gao et al.* [2008]/*Vieira and Solanki* [2010]
GISSC	NASA Goddard Institute for Space Studies [*Schmidt et al.*, 2006]	*Crowley et al.* [2008]/*Vieira and Solanki*, 2010
FGOALS	LASG, Institute of Atmospheric Physics, Chinese Academy of Sciences [*Bao et al.*, 2013; W. Man and T. Zhou, Simulated variability during the past millennium: Results from transient simulation with the FGOALS-s2 climate system model, *Journal of Geophysical Research: Atmospheres*, under revision, 2013]	*Gao et al.* [2008]/*Vieira and Solanki* [2010]
MIROC	Japan Agency for Marine-Earth Science and Technology, Atmosphere and Ocean Research Institute (The University of Tokyo), and National Institute for Environmental Studies [*Watanabe et al.*, 2010]	*Crowley et al.* [2008] / *Delaygue and Bard* [2011] and *Wang et al.* [2005]
MPI	Max Planck Institute for Meteorology [*Raddatz et al.*, 2007; *Marsland et al.*, 2003]	*Crowley et al.* [2008]/*Vieira and Solanki* [2010] and *Wang et al.* [2005]
CCSM4	National Center for Atmospheric Research [*Gent et al.*, 2011]	*Gao et al.* [2008]/*Vieira and Solanki* [2010]
IPSL	Institut Pierre-Simon Laplace [*Marti et al.*, 2010]	*Gao et al.* [2008]/*Vieira and Solanki* [2010] and *Wang et al.* [2005]
CSIRO	The Commonwealth Scientific and Industrial Research Organization [*Phipps*, 2010]	*Crowley et al.* [2008]/*Steinhilber et al.*, [2009]
HadCM3	Hadley Center [*Collins et al.*, 2001]	*Crowley et al.* [2008]/*Steinhilber et al.* [2009]

and Feulner, 2013] have suggested that it is possible to induce long-term cooling given closely spaced multiple volcanic eruptions. *Zhong et al.* [2010] used the National Center for Atmospheric Research Community Climate System Model (CCSM3 model) at T42 resolution to test whether or not a long-term cooling could be induced in the thirteenth century with transient volcanic perturbations. Under particular stability scenarios of the upper North Atlantic (NA) Ocean, the simulations were able to induce abrupt snowline depressions from decadally paced explosive volcanism and sustained expanded snow and ice conditions with sea ice/ocean feedbacks. *Zhong et al.* [2010] found that after the 1257 Samalas eruption, sea surface temperatures (SSTs) in the NA never recovered to their pre-eruption temperatures, as several more large and closely spaced volcanoes erupted and caused cumulative cooling. Cooler NA surface water was then advected to the Atlantic sector of the Arctic Ocean, reducing the rate of basal sea ice melt and allowing sea ice to remain in an expanded state for more than 100 years. *Mignot et al.* [2011] found consistent results for post-thirteenth century eruptions with their model, where they found a weakened Atlantic Meridional Overturning Circulation and a sustained cooling and sea ice expansion in the North Atlantic region. *Schleussner and Feulner* [2013] suggest that an increase in Nordic sea ice extent on decadal timescales as a consequence of major eruptions leads to a spin-up of the subpolar gyre and a weakened Atlantic Meridional Overturning Circulation, eventually causing a persistent basin-wide cooling.

[6] Here, we are interested in how the models from the Paleoclimate Modeling Intercomparison Project Phase 3 (PMIP3) last millennium (LM) simulations compare to paleoclimate reconstructions in the Arctic and NH. We assess whether any of the models produce the reconstructed and previously modeled sustained centennial-scale cold anomalies and expanded sea ice and snow cover in the North Atlantic and Baffin Island regions following multiple, successive large volcanic eruptions.

2. Methods

[7] Seven modeling groups participated in the LM intercomparison project (Table 1). Each group participating ran their coupled atmosphere-ocean model from 850 to 1850 C.E., except Flexible Global Ocean-Atmosphere-Land System (FGOALS), which ran from 1000 to 1999 C.E. The models were forced with volcanic aerosol reconstructions from either *Gao et al.* [2008] or *Crowley et al.* [2008], as outlined in Table 1. Both reconstructions are based on ice core sulfate records from both polar regions and differ in the transfer function from the ice core sulfate to aerosol optical depth (AOD) and in the filtering of globally important eruptions [*Schmidt et al.*, 2011]. There are two Goddard Institute for Space Studies (GISS) simulations, which differ predominantly in their choice of volcanic forcing data set, hereafter referred to as GISSG, which used the *Gao et al.* [2008] reconstruction and GISSC, which used the *Crowley et al.* [2008] reconstruction. Table 1 also notes the solar forcing used in each simulation. *Schmidt et al.* [2011] described the full details of climate forcing reconstruction options for the PMIP3 LM simulations.

[8] Some models did not have snow or ice concentrations available for download. Therefore, we are able to analyze nine unique models for temperature, of which one was GISS which had been run with two different volcanic forcing reconstructions (GISSC and GISSG), seven models for sea ice, and five models for snow.

[9] Due to computational constraints, some of the models were not able to properly spin-up and reach quasi equilibrium. The Model for Interdisciplinary Research on Climate (MIROC) and GISS models show a drift in climate, the former over the entire millennium and the latter over the first 500 years. We address this in the GISS models by removing the linear-fitted trend of the first 500 years of the control run from the forced simulations (GISSG and GISSC) [*Brohan et al.*, 2012] and then adding the climatology of the rest of the control run (the last 500 years) back so we have absolute temperature instead of anomaly. However, for MIROC, since the entire millennial record is drifting, we cannot return to absolute temperature since we do not know the true climate. Thus, we leave MIROC uncorrected. The sea ice and snow in the GISS simulations are corrected in a similar fashion, as is seen, for example, in Figure 5.

[10] Typically, PMIP3 climate model results are compared to proxy records as temperature anomalies, as opposed to absolute temperatures [*Brohan et al.*, 2012; *Landrum et al.*,

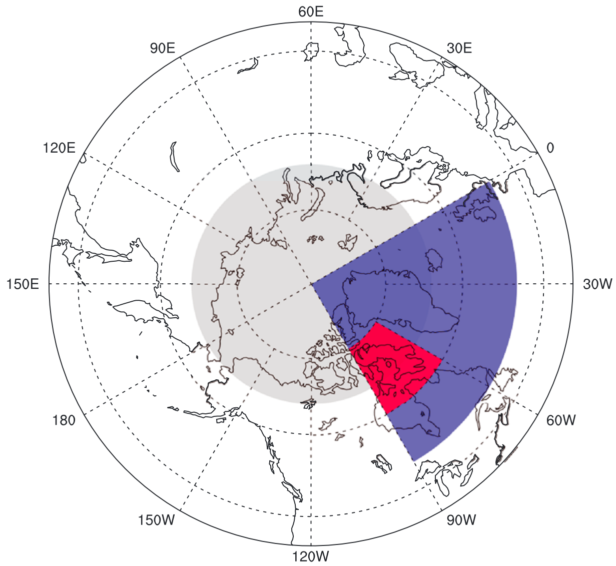

Figure 1. Map showing Arctic region (north of 66°N) in grey, North Atlantic (NA) region (270°W– 360°W, 50°N–90°N) in blue, and the Baffin Island region (270°W–300°W, 60°N–75°N) in red.

2013]. While this method may be appropriate to evaluate variability as relative responses to external forcing, in regions such as the Arctic where temperatures are near the freezing point (and phase changes occur), it is important to report actual temperatures to evaluate the fundamental processes and states of the climate change. Thus, when reporting temperatures in this article, we focus on absolute temperatures intentionally.

[11] We compute area-weighted average temperatures for the Arctic region (north of 66°N), the NA region, and Baffin Island region, shown in Figure 1. Unless otherwise noted (e.g., using land only in these regions or Arctic defined as north of 60°N instead of 66°N), these are the regions referred to in the rest of this article. In some cases we apply a third-order low-pass Butterworth filter as in *Otterå et al.* [2010] so that we retain only multidecadal and slower variability for comparison to proxy reconstructions. To make the model results comparable to sea ice reconstructions, sea ice extent in Figures 4 and 5 is calculated as the areal sum of cells with ice concentration greater than 15%. If the grid cell has a sea ice concentration ≥15%, we consider it to be fully ice covered; otherwise, it is considered ice free, in line with the National Snow and Ice Data Center (NSIDC) sea ice extent definition.

[12] Finally, we perform a superposed epoch analysis (SEA) for our analysis of response to volcanic eruptions. We convert the *Gao et al.* [2008] NH sulfate aerosol loading to aerosol optical depth (AOD) with the conversion factor they recommend of 1.5×10^{14} g. We take the linear average of the *Crowley et al.* [2008] AOD data for the 0°N–30°N and 30°N–90°N latitude bands to generate a NH data set for comparison to *Gao et al.* [2009]. We then find the top 10 volcanic eruptions based on AOD in the NH for both data sets (Table 2). We superpose each eruption event and take the average of their response in temperature, sea ice area, and snow cover area to each major eruption for the 25 years following each event. Each parameter in the SEA analysis is reported as an anomaly with respect to the 5 year average prior to the eruption. Sea ice in the SEA analysis is computed as an area as opposed to extent as in the other calculations in this article. That is, no threshold of 15% is set; instead, we compute the areal sum of the product of grid cell area with ice concentration.

3. Results

3.1. Hemispheric, Arctic, and Regional Temperatures

[13] Figure 2 shows the average June-July-August (JJA) temperature series for the available PMIP3 LM simulations for the Northern Hemisphere, Arctic (north of 66°N), and Baffin Island (land only) region (270°E–300°E, 60°N–75°N). Since we are interested in decadal-scale variability, we used a third-order low-pass Butterworth filter with a cutoff frequency of 15 years [*Otterå et al.*, 2010] to filter the temperature records. The lowest panel shows the *Gao et al.* [2008] NH stratospheric loading of sulfates from volcanic eruptions as an indicator of timing and magnitude of eruptions during the period. A prominent feature of all three temperature panels is the clear difference in mean states for each model, ranging 1.3 K, 2.8 K, and 5.3 K in the NH, Arctic, and Baffin Island, respectively. The order of warmest to coldest model differs depending on the region of interest. Over Baffin Island, the average summer temperatures all tend to be above freezing and those that dip below freezing in posteruption years are CCSM4 and GISSG.

[14] Next, we compare the PMIP3 model results to paleoclimate records in Figure 3. Since the temperature reconstructions are calibrated to instrumental records, there is no large uncertainty in their absolute calibration. All models except MIROC underestimate Arctic-wide JJA near-surface land temperatures. There is better representation by the models of NH annual temperatures, except for the Institut Pierre-Simon Laplace (IPSL) model which underestimates it by several degrees. The GISS models are particularly strong at representing the mean NH climate. These features are also seen in the zonal mean temperatures (not shown) for the NH mean annual and mean JJA temperatures for the full millennium.

[15] The reconstructed temperature response to the eruptions is generally muted compared to almost all of the modeled responses (Figure 3). *Timmreck et al.* [2009] show that the temperature response of the 1257 eruption (and presumably all eruptions) is sensitive to the aerosol particle sizes prescribed in the simulation. They estimate the range of maximum summer NH cooling after the 1257 eruption to be from 0.6 K

Table 2. Top 10 NH Eruptions for the *Gao et al.* [2008] and *Crowley et al.* [2008] Data Sets Based on Aerosol Optical Depth (AOD)

	Gao et al. [2008]		*Crowley et al.* [2008]	
Intensity Rank	Year	AOD	Year	AOD
1	1258	0.97	1258	0.66
2	1783	0.62	1816	0.40
3	1227	0.39	1809	0.29
4	1815	0.39	1641	0.28
5	1600	0.31	1600	0.26
6	1176	0.31	1228	0.18
7	1452	0.30	1460	0.15
8	1641	0.23	1668	0.15
9	939	0.21	1585	0.14
10	1719	0.21	1024	0.14

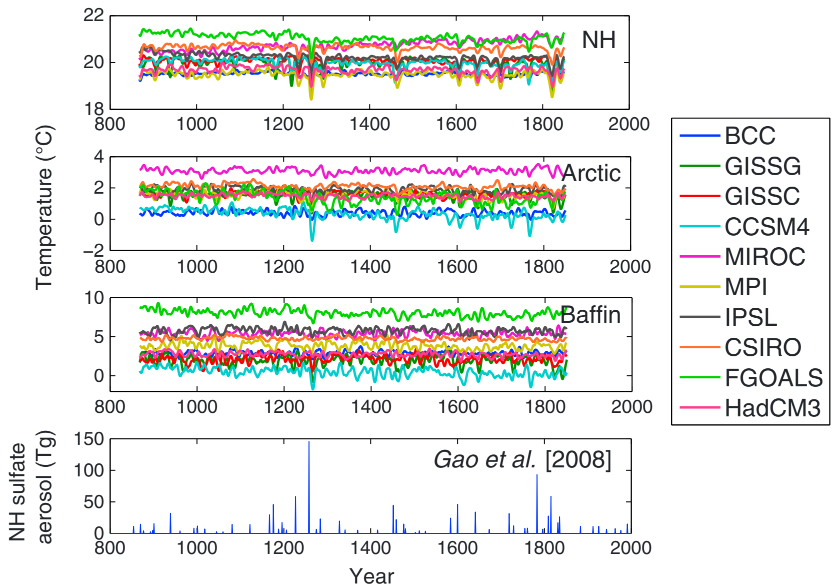

Figure 2. JJA temperature time series for each last millennium model simulation for the Northern Hemisphere, Arctic (north of 66°N) land and ocean, and Baffin Island (land only). Data are filtered with a third-order low-pass Butterworth filter with a cutoff frequency of 15 years. The bottom panel shows the total Northern Hemisphere stratospheric sulfate aerosol ejection (Tg) [*Gao et al.*, 2008]. GISS models have been corrected for drift in the first 500 years.

to 2 K. They show that only aerosol particle sizes substantially larger than observed after Pinatubo yield temperature responses consistent with reconstructions. The *Gao et al.* [2008] reconstruction contains no information about particle size distribution, and the *Crowley et al.* [2008] data set includes uncertain estimates of particle size, so using the wrong size distribution may be the reason that the temperature response in the models to the 1257 eruption, and others, is overestimated. The magnitude of response in the Arctic and the NH after the 1257 eruption (Figure 3) is comparable

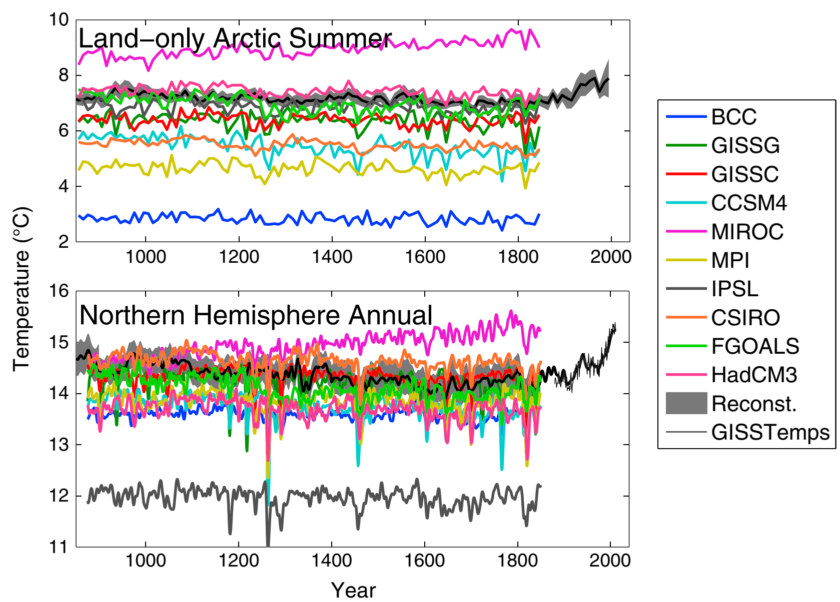

Figure 3. Comparison of paleoclimate temperature reconstructions to PMIP3 for the (top) Arctic summer (JJA) land-only north of 60°N and (bottom) NH annual temperature reconstruction. GISS models have been corrected for drift in the first 500 years. Arctic reconstruction is from *Kaufman et al.* [2009] and compared to PMIP3 decadal averages. NH reconstruction is from *Mann et al.* [2009] and compared to 10 year low-pass Butterworth filtered PMIP3 data. GISS temperatures are derived from land and ocean station temperature anomalies for the NH from http://data.giss.nasa.gov/gistemp/. They were then converted to absolute temperature with the *Jones et al.* [1999] 1961–1990 base period average (14.6°C).

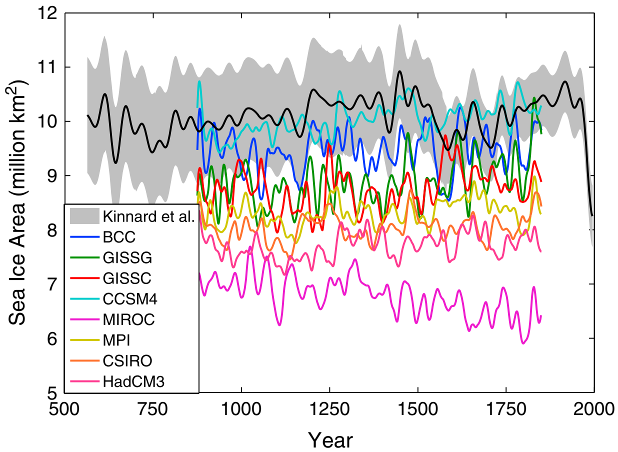

Figure 4. NH late summer (August) sea ice extent (millions km^2) for PMIP3 simulations filtered with a third-order Butterworth 40 year low-pass filter compared to *Kinnard et al.* [2011] 40 year smoothed reconstruction of sea ice extent based on 69 proxy records. GISS models are corrected for first 500 years of drift. PMIP3 models calculated using 15% ice cover threshold (any cell ≥15% ice cover is considered fully covered, whereas anything <15% cover is considered open ocean).

between the GISSG than the GISSC simulations, although this is not the case for other major eruptions throughout the simulations. Further error sources, such as location of the volcano and season of eruption, complicate matters even more [*Anchukaitis et al*., 2012; *Toohey et al*., 2011]. In their assessment of the CCSM4 LM simulation, *Landrum et al.* [2013] found the response of the model to large eruptions to be 2–3 times larger than the NH anomalies estimated from tree rings. The twentieth century response to volcanic eruptions is also noted to be too strong [*Meehl et al*., 2012]. Indeed, errors in the paleoclimate reconstructions are very possible as well. *Mann et al*. [2012] suggested that NH volcanic responses were being underestimated by tree ring-based reconstructions, although there has been opposition to this suggestion [*Anchukaitis et al*., 2012].

[16] Lastly, we assess whether or not the models are able to reproduce a sustained Arctic LIA cooling. Proxy records suggest that NH temperatures decreased by roughly 0.5 K [*Mann et al*., 2009] and that at least a regional summer temperature lowering of 2 or 3 K occurred in the North Atlantic sector of the Arctic [*Miller et al*., 2012]. We test whether the models produce an Arctic and Baffin Island cooling with LIA period definition of 1450–1850 and 1600–1850. We compare this to the periods 850–1450 and 850–1600, respectively. We find that all models (except MIROC with the LIA defined as 1450–1850) produce statistically significant colder summer Arctic average temperatures (based on a Student's *t* test), no matter which period is defined as the LIA. The maximum cooling is 0.3 K in the CCSM4 model. All other models produce less than 0.2 K change. We do the same analysis for Baffin Island summer land temperatures and find that four models produce statistically significant colder temperatures in the LIA than in the period before. The maximum cooling achieved is again by the CCSM4 model, of 0.5 K. Thus, the LIA is generated in most models, but its magnitude is very weak compared to what proxy records suggest.

3.2. Sea Ice

[17] Despite the issues with model resolution and snow cover representation on Baffin Island, another measure of multidecadal model response to repeated volcanic forcing is in the sea ice. *Miller et al*. [2012] cite an ocean/sea ice feedback mechanism by which a centennial-scale expansion of snow cover and sea ice is maintained. Here, we assess whether any of the PMIP3 models show a sustained sea ice expansion in the North Atlantic region.

[18] First, we compare the PMIP3 NH sea ice extent to the *Kinnard et al*. [2011] Arctic August sea ice extent reconstruction, which is based on 69 proxies predominantly derived from ice cores, but also from tree rings, lake sediments, and historical observations of sea ice. The reconstruction was calibrated against an historical index of late-summer extents (at least 15% concentration) from 1870–1995. All PMIP3 model ice extents are calculated with a 15% concentration threshold as well, consistent with the paleoclimate reconstruction and NSIDC methodology, where any grid cell with ≥15% ice concentration is considered fully covered; otherwise, it is considered ice free. Aside from CCSM4 and the Beijing Climate Center (BCC) model, which largely fall within the reconstruction uncertainty range, the models tend to underestimate the sea ice extent for the duration of the last millennium (Figure 4). The correlation of the models with reconstruction is usually significant (p values of < 0.05 using Student's t test), but in seven of the eight runs, it is negative. MIROC shows the least sea ice area, although it is the only model to positively correlate with the reconstruction. We did not find any consistent lags between individual models or between models and reconstructions.

[19] The CCSM4 simulation shows a period of generally higher sea ice extent between about 1250 and 1500 C.E., suggesting that this model has a multidecadal sea ice response after the 1257 eruption. Figure 5 shows the minimum annual sea ice extent in the NA region for each model. The 40 year low-pass filtered time series exceeds the standard deviation of the low volcanic activity reference period (850–1150 C.E.) only in the GISSG, GISSC, and CCSM4 models. The significant (>1σ) expansion of sea ice in these models lasts up to a few decades in GISSG and GISSC, and up to 80 years in CCSM4, but never reaches a continuous centennial long expansion. Analysis of SSTs (not shown) in a subset of the North Atlantic (50°W–20°W and 50°N–65°N, per *Zhong et al*. [2010]) shows that none of the models produce a cumulative cooling after the 1257 Samalas and the subsequent closely spaced eruptions. This was a key step in the mechanism for sustaining sea ice in the volcanically perturbed thirteenth century [*Miller et al*., 2012; *Zhong et al*., 2010]. As a result, we infer that the rate of basal sea ice melt in the Arctic Ocean was not reduced, and thus, sea ice did not remain in an expanded state for more than 100 years.

3.3. Model Elevation

[20] We suspect that model resolution plays a factor in properly representing the mean climate over Baffin Island, whose highest peak in reality, Mount Odin, reaches over 2 km above sea level. Figure 6a shows the model representation and actual Baffin Island topography, along with the number of grid cells (n) comprising the Baffin Island region. Actual elevations are derived from the U.S. Geological Survey GTOPO30 product, available from http://earthexplorer.usgs.gov/. This digital

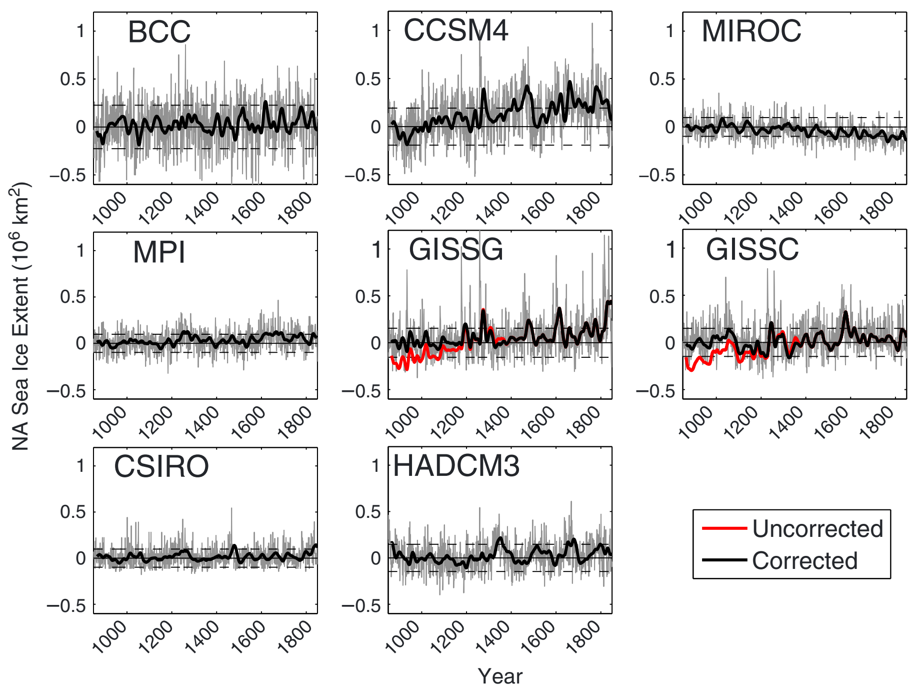

Figure 5. Anomaly of minimum annual North Atlantic sea ice extent (grey) overlain with 40 year low-pass filtered series (black) with respect to the reference period 850–1150 C.E. (a time with low volcanic activity). Dashed lines show standard deviation of sea ice extent of reference. Models do not show centennial-scale expanded sea ice in this region after multiple closely spaced eruptions in the late thirteenth century. Sea ice extent is calculated with a 15% grid cell coverage threshold for full ice cover versus open ocean, and the drift-corrected and uncorrected GISS curves are shown.

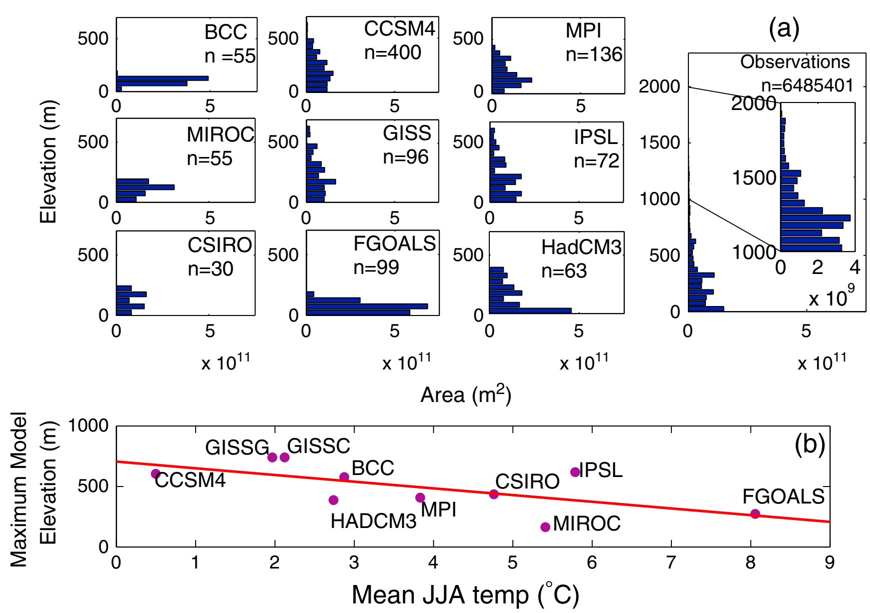

Figure 6. (a) Histograms of Baffin Island grid cell elevation distribution in terms of area represented for each model and the observed digital elevation retrievals from the GTOPO30 data set (http://earthexplorer.usgs.gov/). The GTOPO30 observations panel inset emphasizes the high elevations present in reality on Baffin Island. Number of grid cells in the Baffin Island region is denoted with *n*. Few models represent the Baffin Island plateau elevation range of 400–700 m, critical to snow expansion and persistence. (b) Maximum model elevation as a function of mean model summer (JJA) 2 m temperature over Baffin Island land from 850–1850 C.E. The red curve shows the best fit linear regression. There is a relationship between maximum summer temperatures and the model topography of the island. GISS models have been corrected for drift in the first 500 years.

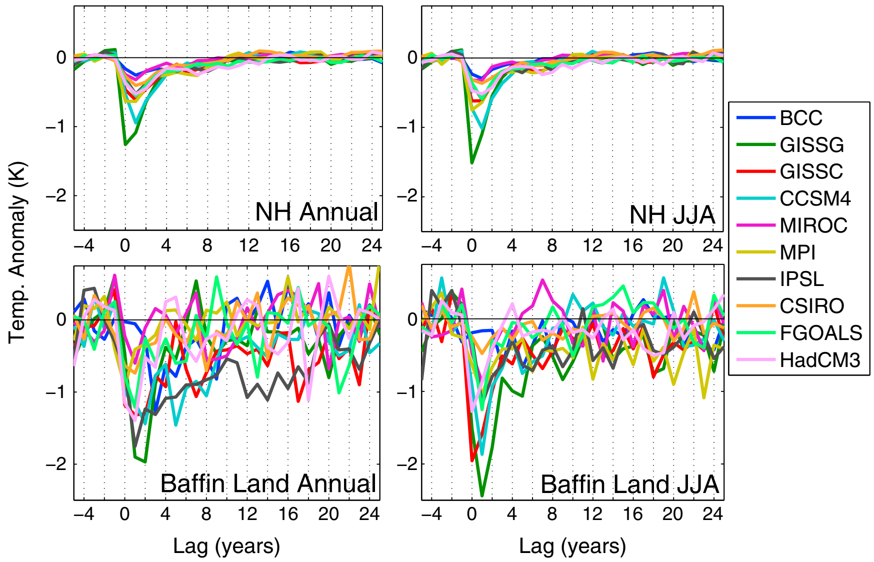

Figure 7. Superposed epoch analysis of NH annual, summer (JJA), Baffin Island (land only) annual, and JJA average temperature response to the top 10 eruptions in the last millennium. Anomaly is relative to the 5 year average before eruptions. GISS models have been corrected for drift in the first 500 years.

elevation model has a resolution of 30 arcseconds, which roughly equates to 1 × 1 km grids at the equator that get smaller toward the poles. The representation of elevations above 400 m is deficient in most models compared to the GTOPO30 data (Figure 6a). None of the models represents elevations above 750 m, while in reality, more than 500 km^2 of the region resides at higher elevations. The lack of representation of these high elevations in the models would not only have impacts on snow and ice, but also on atmospheric circulation. We examine the relationship between maximum model elevation and mean summer (JJA) surface temperature in Figure 6b. Models with higher peak elevations on Baffin Island tend to have colder mean summer climates. The two models with the coldest climate in the Baffin Island region, CCSM4, and GISS, also represent the high plateaus (400–700 m) [*Andrews et al.*, 1972], elevations critical in fostering and sustaining large snow area change [*Berdahl and Robock*, 2013].

3.4. Model Response to Volcanic Eruptions in the Last Millennium

[21] The results of our SEA analysis for temperature, sea ice, and snow cover with the top 10 eruptions in the last millennium are described below.

3.4.1. Temperature

[22] We analyze the response of the mean NH JJA and annual temperatures as well as those over Baffin Island land only (Figure 7). In all cases, the GISSG model shows the strongest average peak response exceeding 1 K NH annual average cooling and becomes even greater in the summer months reaching roughly 1.5 K. All models show a post-eruption cooling, MIROC being the most muted in the NH.

[23] The temperature response on Baffin Island is again strongest in the GISSG simulation, in both annual and summer averages. Summertime average responses mainly govern the minimum snow cover extent on the island. Baffin Island summer temperatures cool by over 2 K in the GISSG model, followed by GISSC and CCSM4. The MIROC and BCC models show mild and slightly delayed post-eruption temperature decreases compared to that of the GISS and CCSM4 models. The GISSG model shows the slowest recovery in the first 5 post-eruption years, although the Max Planck Institute (MPI) model shows similar cooling in the decades following the eruption even though it does not reach such extreme cooling in year 1.

[24] The integrated temperature response per unit forcing from year 0 to year 10 is shown in Table 3 for NH and Baffin Island annual and JJA average responses for the top 10 eruptions. The models with the largest integrated NH annual and JJA temperature response are MPI, Hadley Coupled Model (HadCM3), and the GISS model. On Baffin Island, the integrated annual temperature response is strongest in MPI and the GISS models, whereas in the summer, the GISS, IPSL, and CCSM4 show the strongest net cooling in the 10 years following the eruptions. Thus, the model temperature responses do not rank consistently from region to region or season to season, and their impact on the cryosphere is not only dependent on the temperature anomalies but also on the mean state of the background climate.

3.4.2. Sea Ice

[25] The SEA analysis for September sea ice area in the NH and the NA regions (Figure 8) follows that of temperature. In the NH, GISSG shows a significantly larger response than any of the other models, more than twice the area anomaly than any other model. All models subside to pre-eruption conditions by 10 years after the eruption. In the NA, GISSG shows the largest peak in sea ice area anomaly after the eruptions, although it is followed closely by CCSM4, GISSC, and BCC. Again, the anomalies subside within roughly a 10 year lag of the eruption.

[26] Integrated sea ice area expansion per unit forcing for 10 years following the eruptions is shown for the NH and NA in Table 3. In the NH, sea ice expansion is largest per unit forcing in the GISS models and HadCM3. In the North Atlantic, the GISS models and CCSM4 produce the greatest integrated sea ice expansion in the 10 years following the eruptions. Again, over Baffin Island, the coldest models are

Table 3. Temperature, Sea Ice, and Snow Anomaly Responses Per Unit Forcing (UF) Integrated From Year 0 to Year 10 Lag After the Eruption

Model	NH Annual Temperature (K/UF)	NH JJA Temperature (K/UF)	Baffin Annual Temperature (K/UF)	Baffin JJA Temperature (K/UF)	NH Sea Ice Area ($\times 10^6$ km^2/UF)	NA Sea Ice Area ($\times 10^6$ km^2/UF)	NH Snow Area ($\times 10^6$ km^2/UF)	Baffin Snow Area ($\times 10^6$ km^2/UF)
BCC	−3.5	−2.6	−8.4	−12.4	16.0	3.4	2.0	0.1
GISSG	−10.4	−10.2	−25.1	−40.9	24.1	5.3	9.8	3.0
GISSC	−10.2	−9.6	−57.6	−48.4	20.8	4.8	5.5	1.9
CCSM4	−8.4	−8.2	−35.1	−18.4	7.1	3.5	9.5	3.1
MIROC	−5.0	−4.1	−3.8	−7.6	13.5	1.8	3.3	0.0
MPI	−11.9	−10.9	−1.5	−49.9	14.8	1.8	0.2	0.0
IPSL	−6.4	−6.2	−51.1	−28.1				
CSIRO	−7.2	−6.3	−9.6	−10.9	10.5	2.1		
FGOALS	−6.4	−5.7	−15.5	−6.0				
HadCM3	−10.7	−10.2	−20.9	−20	16.8	2.6		

[a]Average forcing for the top 10 eruptions in terms of aerosol optical depth (Table 2) is used to compute response per UF. Anomalies are calculated from the 5 year pre-eruption climatology. A 10 year pre-eruption climatology was tested as well but made minimal difference to the results.

CCSM4 and GISS, so it follows that they would produce the most sea ice in this region.

3.4.3. Snow

[27] The SEA analysis for snow is shown for the Baffin region and the NH, expressed as a percentage of land covered in snow at the annual minimum of monthly mean extent (typically August) and as a snow area anomaly with respect to the mean of 5 years prior to the eruptions (Figure 9). The minimum annual percent of snow cover on land in the NH varies across the models with CCSM4 differing from MIROC NH snow cover by 3% (more than 150% change). In other words, the mean minimum annual snow extent in the MIROC model covers about 3.0×10^6 km^2 less in area than that of the CCSM4 model. As discussed earlier, this is probably in part a function of model resolution since higher-resolution models can capture higher elevations that are colder and sustain snow cover. The post-eruption snow extent anomaly in the NH is strongest and very similar in the GISSG and the CCSM4 models. This response tapers off within a decade in all models, earlier in most.

[28] On Baffin Island, the story is similar. The MIROC model shows minimal snow retention at the peak of summer on the island and no significant post-eruption anomaly even after the eruptions in this region. The BCC and MPI models produce a similar result, although their minimum snow extent tends to be higher. The CCSM4, GISSG, and GISSC models show significant responses to the eruptions on Baffin Island, both in terms of percentage and area anomaly. The CCSM4 and GISSG models show the same maximum area anomaly over Baffin Island, roughly twice the magnitude of that seen in GISSC. Similar to the NH, the post-eruption snow expansion is short-lived, decaying back to pre-eruption snow extents within 10 years.

[29] Table 3 shows the NH and Baffin Island snow area anomalies following the top 10 eruptions integrated over lag years 0 to 10. In both cases, the snow expansion is largest in

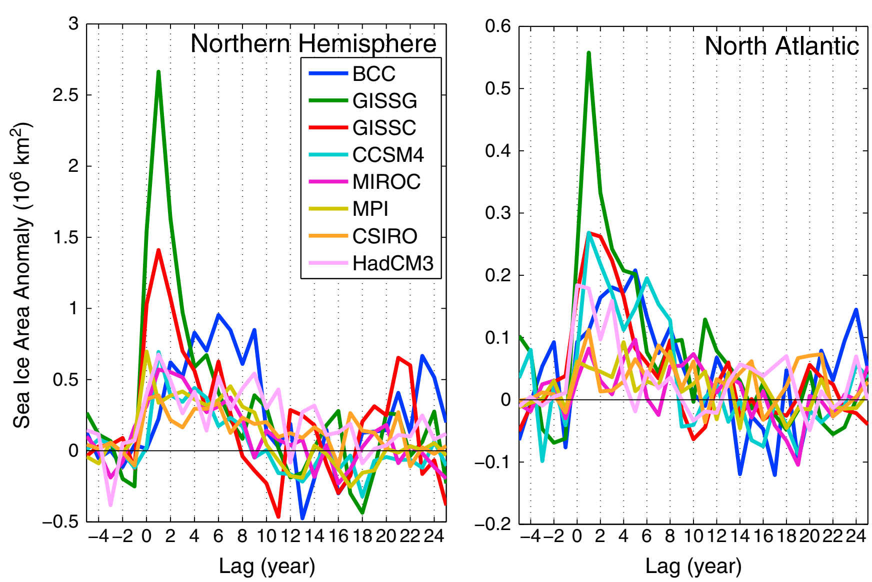

Figure 8. Superposed epoch analysis for top 10 eruptions in the last millennium (Table 2), showing Northern Hemisphere and North Atlantic September sea ice area. Anomaly is with respect to the mean of 5 years prior to the eruptions. Note on the different scales on the *y* axis. GISS models are corrected for the first 500 years of drift.

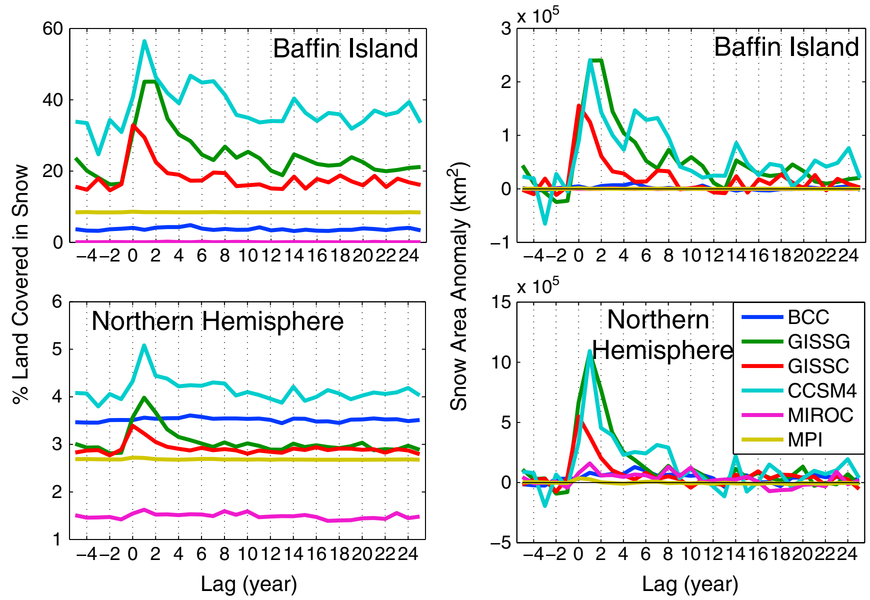

Figure 9. Superposed epoch analysis for the top 10 eruptions in the last millennium (Table 2). Panels show snow area coverage in the Baffin Region (270°W–300°W, 60°N–75°N) and for the Northern Hemisphere expressed as the percent of the total land area covered in snow at the minimum annual extent in the left panels. The right panels show the snow area anomaly with respect to the mean of the 5 years prior to the eruptions for the same regions. Lag of 0 represents the year of the eruption. Note on the different scales on the *y* axes. GISS models have been corrected for drift in the first 500 years.

the GISS and CCSM4 models. Over Baffin Island, the largest integrated response is generated by the CCSM4 and the GISSG model. Again, these are the coldest models in this particular region, although these models rank only third and fourth in their summer temperature response to the eruptions over Baffin Island. This emphasizes that both the background summer climate and the strength of the response to volcanic eruptions simulated by the models

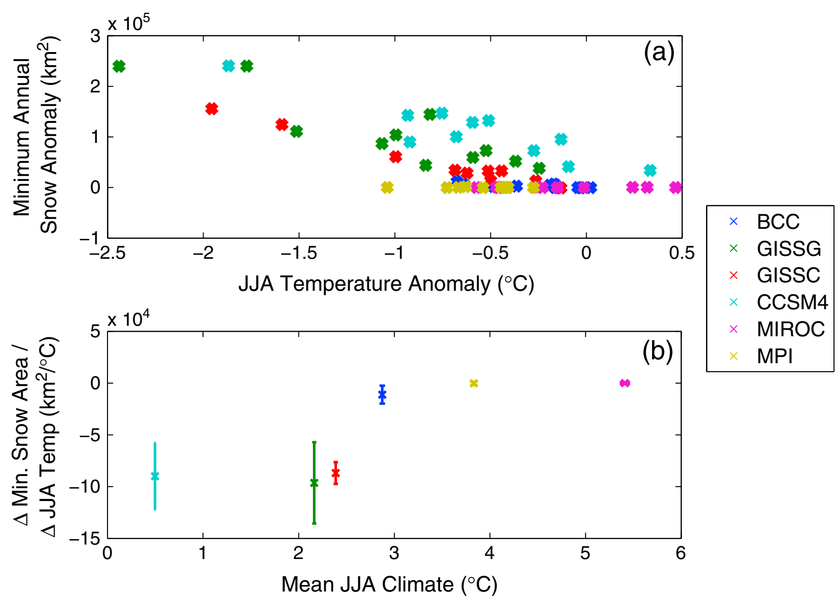

Figure 10. SEA minimum annual Baffin Island snow cover anomaly as a function of SEA JJA temperature anomaly for the 10 years following the top 10 eruptions (lag years 1–10 in Figures 9 and 7, respectively). Anomalies are with respect to the SEA values for the 5 years prior to the eruptions (lag years −5 to −1 in Figures 9 and 7). GISS models have been corrected for the first 500 years of drift. (a) Ordinate value is calculated as the slope for each model. (b) Magnitude of snow cover expansion on Baffin Island during summer cooling after the top 10 eruptions, plotted against the mean JJA Baffin Island climate for each model. Error bars show 95% confidence level. GISS models previously corrected for the first 500 years of drift.

dictate the behavior of the cryosphere. This is in agreement with the general conclusions of *Zanchettin et al*. [2013].

3.4.4. Model Sensitivity

[30] Next, we assess the SEA temperature and snow responses together, by plotting the temperature and snow SEA time series against each other (Figure 10a). We truncate the time series to include only lag year 1 to lag year 10 since we are interested in post-eruption response. From this we can fit least-squares regression fits to each model and find the sensitivity of the snow response to temperature change for each model (units of km^2/K). Plotting these sensitivities against the mean JJA climate in each model over Baffin Island, we show that the models' ability to produce a snow response is strongly a function of the mean climate (Figure 10b). There is a sudden transition between models exhibiting a widespread change in snow cover and those with virtually no change in snow. Above about 2.5°C mean summer climate, the models become incapable of reaching the freezing point and forming snow, let alone sustaining extra amounts of snow on Baffin Island. Below roughly 2.5°C, the models show widespread snow expansion. The temperature response after the eruption is also a function of the volcanic reconstruction used, which is evident in the GISS models, whose primary difference is the choice of volcanic forcing reconstruction. This result highlights the necessity for models to not just correctly reproduce eruption response as anomalies, but equally important, they must be able to capture the absolute temperature. This has particularly critical consequences around the freezing mark, as the presence of snow and ice triggers the ice-albedo feedback, one of the most important climate feedbacks on the globe.

4. Discussion

[31] We can summarize our main findings as follows. Comparison of NH, Arctic, and Baffin Island temperature in the PMIP3 models shows a large spread in mean model background climate, the rank of which is not consistent across regions. Annual average NH mean climates span 3 K, Arctic average summer temperatures span 3 K, and Arctic land-only summer climates range by more than 6 K. Over Baffin Island, summer temperatures dip below 0°C after major eruptions only in the GISSG, GISSC, and CCSM4 simulations, allowing snow to expand on the island only in these models despite other models having a greater integrated temperature response per unit forcing. Mean summer climate of Baffin Island is partly a function of the model resolution and grid cell elevations. Most models produce a Little Ice Age; however, the magnitude of associated cooling is much less than expected from reconstructions. The largest change noted was about 0.5 K cooling on Baffin Island, compared to the proxy data which suggests that at least several degrees of cooling occurred [*Miller et al*., 2012]. The temperature response to volcanic eruptions is generally stronger in the PMIP3 models than in reconstructions, consistent with other studies [*Landrum et al*., 2013; *Brohan et al*., 2012; *Meehl et al*., 2012]. This could be a result of, for example, inadequate aerosol representation [*Timmreck et al*., 2010], model difficulty in capturing dynamic responses in the stratosphere [*Shindell et al*., 2003], uncertainties in eruption location and time of year [*Anchukaitis et al*., 2012; *Toohey et al*., 2011], and potential errors in ice core interpretation when generating volcanic reconstructions [*Schneider et al*., 2009]. Problems with the paleoclimate reconstructions are of course possible as well. It has been suggested that there is an underestimation of volcanic cooling in tree ring-based reconstructions of Northern Hemisphere temperature [*Mann et al*., 2012], although this has been vehemently rebutted by others [*Anchukaitis et al*., 2012].

[32] Sea ice extent tends to be underestimated in most of the models compared to the *Kinnard et al*. [2011] reconstruction. CCSM4 and BCC do well in their sea ice extent representation, falling within the range of uncertainty of the reconstruction. Compared to the period 850–1150 C.E. which is characterized by low volcanic activity, 40 year low-pass filtered sea ice area in the NA shows decadal-scale expansion occasionally after the mid-thirteenth century in the GISSG, GISSC, and CCSM4 models, but does not show centennial-scale expansion in the LM simulations. The key event in the *Miller et al*. [2012] modeling was volcanic activity in the late thirteenth century. At that time, eruptions were closely spaced enough that the North Atlantic surface waters never recovered to their pre-eruption temperature between eruptions, so that there was a cumulative temperature lowering larger than for any single volcanic event. Our analysis of SSTs in the PMIP3 models (not shown) in a subdomain of the North Atlantic (50°W–20°W and 50°N–65°N, per *Zhong et al*. [2010]) do not produce a sustained cooling beyond about a decade after the 1257 Samalas eruption. The relatively warm SST conditions in the PMIP3 simulations likely contribute to limiting the sea ice expansion during the thirteenth century.

[33] The SEA analysis reveals the temperature response to SVEs in the NH is strongest in the GISSG model, with more than 1 K maximum annual average cooling and up to 1.5 K maximum summer average cooling. MIROC and BCC show less than 0.5 K maximum cooling for both annual and summer cooling. Cooling is much stronger over Baffin Island land, particularly in the summer, when GISSG exceeds 2 K cooling, and greater than 1 K cooling is produced in all other models except BCC and MIROC. Minimum annual sea ice area expands most in GISSG, and this behavior is especially outstanding from the other models in the NH compared to the NA. On average, CCSM4 produces the most expansive minimum annual NH snow cover, followed by the BCC, GISS, MPI, and MIROC models. The only models that show a response in the SEA snow analysis in the NH and over Baffin Island are GISSG, CCSM4, and GISSC models. Over Baffin Island, the largest integrated response in snow area from year lag 0 to 10 is in CCSM4 and GISSG. Again, these are the coldest models in this region, although these models rank only third and fourth in their integrated summer temperature response to the eruptions over Baffin Island. Thus, a combination of appropriate background climate and response to volcanic eruptions is necessary to generate a response in the cryosphere, in agreement with the findings in *Zanchettin et al*. [2013]. From the SEA snow and temperature analyses over Baffin Island, we find that the only models that manifest a snow expansion in response to a temperature drop after SVEs are the models whose mean summer climates are near enough to 0°C, such that a perturbation brings temperatures below freezing. There is a sharp transition between the degree of snow expansion in models with a mean climate below and above about 2.5°C. *Zhong et al*. [2010] and *Miller et al*. [2012] used CCSM3, CCSM4's

predecessor, to produce a centennial-scale climate change from decadally paced SVEs. Here we show that the coldest model in the Baffin Island region is CCSM4, so it is likely that CCSM3 also produces near-zero temperatures in this region. It is possible, then, that they may not have found significant and sustained sea ice and snow expansion if they had used a climate model which happened to model a warmer mean state in this region. Ultimately, we show that it is critical to accurately model the absolute temperature in regions near the freezing point where snow and ice form and melt. Crossing this threshold could potentially induce feedback that support further sea ice expansion, colder SSTs, and consequently colder and snowier conditions on land.

5. Conclusions

[34] We assessed the PMIP3 LM simulations in terms of absolute temperatures and the temperature, snow, and ice response to volcanic eruptions with a focus on the North Atlantic and eastern Canadian Arctic regions in order to determine if current state-of-the-art models produce sudden and persistent cold conditions after SVEs. We have shown that the PMIP3 models are generally colder than reconstructions over Arctic land but at the same time have too little sea ice in the Arctic compared to reconstructions. Most models produce significantly cooler temperatures in the Arctic and in the North Atlantic region during the LIA; however, the magnitude of cooling is much less than expected from proxy records. Only two of the models produce decadal sea ice expansion, but none produce centennial-scale expansion. Snow cover over Baffin Island shows large-scale expansion in only two of the five available models, although it is not sustained beyond a decade. The PMIP3 models' lack of sustained cooling response could be due to their inability to capture changes in ocean circulation, which other studies have shown can lead to centennial-scale cooling in the North Atlantic.

[35] Spread in the models' mean climate states in the NH, Arctic, and over Baffin Island is evident. Model resolution, and consequently topography, plays a strong role in determining mean climate over Baffin Island. Critical plateau elevations of 400–700 m, necessary for fostering and sustaining large snow area change [*Berdahl and Robock*, 2013], are only represented in the CCSM4 and GISS models. In more than half of the models, warm summer climates over Baffin Island stunt snow expansion after volcanic eruptions completely. Thus, it is crucial to properly represent absolute temperatures particularly in areas such as the Arctic where small temperature changes dictate phase changes of water. This is especially important, since snow and ice presence can further induce feedback, such as ice-albedo, which may influence global climate but cannot be triggered from volcanic forcing in models that are too warm.

[36] **Acknowledgments.** We thank Giff Miller, Davide Zanchettin, and an anonymous reviewer for their thoughtful comments on this paper, which very much improved this manuscript. We thank Philip Brohan and Johann Jungclaus for sharing valuable insight regarding the PMIP3 models and Reto Ruedy for help with GISS temperatures. We acknowledge all of the modeling groups in the PMIP project for producing and making available their results through the Earth Systems Grid Federation archive. This work was supported by NSF grants ARC-0908834 and AGS-1157525.

References

Anchukaitis, K. J., et al. (2012), Tree rings and volcanic cooling, *Nat. Geosci.*, *5*(12), 836–837.

Andrews, J. T., R. G. Barry, R. S. Bradley, G. H. Miller, and L. D. Williams (1972), Past and present glaciological responses to climate in eastern Baffin Island, *Quat. Res.*, *2*(3), 303–314.

Bao, Q., et al. (2013), The flexible global ocean-atmosphere-land system model, spectral version 2: FGOALS-s2, *Adv. Atmos. Sci.*, *30*, 561–576.

Berdahl, M., and A. Robock (2013), Baffin Island snow extent sensitivity: Insights from a regional climate model, *J. Geophys. Res. Atmos.*, *118*, 3506–3519, doi:10.1002/jgrd.50249.

Briffa, K. R., P. D. Jones, F. H. Schweingruber, and T. J. Osborn (1998), Influence of volcanic eruptions on Northern Hemisphere summer temperature over the past 600 years, *Nature*, *393*, 450–455, doi:10.1038/30943.

Brohan, P., R. Allan, E. Freeman, D. Wheeler, C. Wilkinson, and F. Williamson (2012), Constraining the temperature history of the past millennium using early instrumental observations, *Clim. Past*, *8*, 1551–1563, doi:10.5194/cp-8-1551-2012.

Collins, M., S. F. B. Tett, and C. Cooper (2001), The internal climate variability of HadCM3, a version of the Hadley Centre Coupled Model without flux adjustments, *Clim. Dyn.*, *17*(1), 61–81.

Crowley, T. J., G. Zielinski, B. Vinther, R. Udisti, K. Kreutzs, J. Cole-Dai, and E. Castellano (2008), Volcanism and the Little Ice Age, *PAGES Newslett.*, *16*, 22–23.

Delaygue, G., and E. Bard (2011), An Antarctic view of Beryllium-10 and solar activity for the past millennium, *Clim. Dyn.*, *36*, 2201–2218, doi:10.1007/s00382-010-0795-1.

Frank, D. C., J. Esper, C. C. Raible, U. Buentgen, V. Trouet, B. Stocker, and F. Joos (2010), Ensemble reconstruction constraints on the global carbon cycle sensitivity to climate, *Nature*, *463*, 527–530, doi:10.1038/nature08769.

Gao, C., A. Robock, and C. Ammann (2008), Volcanic forcing of climate over the past 1500 years: An improved ice core-based index for climate models, *J. Geophys. Res.*, *113*, D23111, doi:10.1029/2008JD010239.

Gent, P. R., et al. (2011), The Community Climate System Model version 4, *J. Clim.*, *24*, 4973–4991, doi:10.1175/2011JCLI4083.1.

Hegerl, G. C., T. Crowley, M. Allen, W. T. Hyde, H. Pollack, J. Smerdon and E. Zorita (2007), Detection of human influence on a new 1500 yr climate reconstruction, *J. Climate*, *20*, 650–666.

Jansen, E., et al. (2007), Palaeoclimate, in *Climate Change 2007: The Physical Science Basis—Contribution of Working Group I to the Fourth Assessment Report of the Intergovernmental Panel on Climate Change*, edited by S. Solomon et al., pp. 463–497, Cambridge Univ. Press, Cambridge, U.K.

Jones, P. D., M. New, D. E. Parker, S. Martin, and I. G. Rigor (1999), Surface air temperature and its change over the past 150 years, *Rev. Geophys.*, *37*, 173–199.

Kaufman, D. S., et al. (2009), Recent warming reverses long-term Arctic cooling, *Science*, *325*(5945), 1236–1239.

Kinnard, C., C. M. Zdanowicz, D. A. Fisher, E. Isaksson, A. de Vernal, and L. G. Thompson (2011), Reconstructed changes in Arctic sea ice over the past 1,450 years, *Nature*, *479*(7374), 509–512.

Landrum, L., B. L. Otto-Bliesner, E. R. Wahl, A. Conley, P. J. Lawrence, N. Rosenbloom, and H. Teng (2013), Last millennium climate and its variability in CCSM4, *J. Clim.*, *26*, 1085–1111, doi:10.1175/JCLI-D-11-00326.1.

Langway, C. C., Jr., K. Osada, H. B. Clausen, C. U. Hammer, and H. Shoji (1988), An inter-hemispheric volcanic time-marker in ice cores from Greenland and Antarctica, *Ann. Glaciol.*, *10*, 102–108.

Lavigne, F., et al. (2013), Source of the great A.D. 1257 mystery eruption unveiled, Samalas volcano, Rinjani Volcanic Complex, Indonesia, *Proc. Natl. Acad. Sci. U. S. A.*, doi:10.1073/pnas.1307520110, in press.

Mann, M. E., Z. Zhihua, M. K. Hughes, R. S. Bradley, S. K. Miller, S. Rutherford, and F. Ni (2008), Proxy-based reconstructions of hemispheric and global surface temperature variations over the past two millennia, *Proc. Natl. Acad. Sci. U.S.A.*, *105*(36), 13,252–13,257, doi:10.1073/pnas.0805721105.

Mann, M. E., Z. Zhang, S. Rutherford, R. S. Bradley, M. K. Hughes, D. Shindell, C. Ammann, G. Faluvegi, and F. Ni (2009), Global signatures and dynamical origins of the Little Ice Age and Medieval Climate Anomaly, *Science*, *326*(5957), 1256–1260.

Mann, M. E., J. D. Fuentes, and S. Rutherford (2012), Underestimation of volcanic cooling in tree-ring-based reconstructions of hemispheric temperatures, *Nat. Geosci.*, *5*, 202–205, doi:10.1038/NGEO1394.

Marsland, S. J., H. Haak, J. H. Jungclaus, M. Latif, and F. Roeske (2003), The Max-Planck-Institute global ocean/sea ice model with orthogonal curvilinear coordinates, *Ocean Modell.*, *5*, 91–127.

Marti, O., et al. (2010), Key features of the IPSL ocean atmosphere model and its sensitivity to atmospheric resolution, *Clim. Dyn.*, *34*, 1–26.

Meehl, G. A., et al. (2012), Climate system response to external forcings and climate change projections in CCSM4, *J. Climate*, *25*, 3661–3683, doi:10.1175/JCLI-D-11-00240.1.

Mignot, J., M. Khodri, C. Frankignoul, and J. Servonnat (2011), Volcanic impact on the Atlantic Ocean over the last millennium, *Clim. Past*, *7*, 1439–1455, doi:10.5194/cp-7-1439-2011.

Miller, G. H., et al. (2010), Temperature and precipitation history of the Arctic, *Quat. Sci. Rev.*, *29*(15–16), 1679–1715, doi:10.1016/j.quascirev.2010.03.001.

Miller, G. H., et al. (2012), Abrupt onset of the Little Ice Age triggered by volcanism and sustained by sea-ice/ocean feedbacks, *Geophys. Res. Lett.*, *39*, L02708, doi:10.1029/2011GL050168.

Otterå, O. H., M. Bentsen, H. Drange, and L. Suo (2010), External forcing as a metronome for Atlantic multidecadal variability, *Nat. Geosci.*, *3*, 688–694.

Phipps, S. J. (2010), The CSIRO Mk3L climate system model v1.2, Technical Report No. 4, Antarctic Climate & Ecosystems CRC, Hobart, Tasmania, Australia, 122 pp., ISBN 978-1-921197-04-8.

Raddatz, T. J., C. H. Reick, W. Knorr, J. Kattge, E. Roeckner, R. Schnur, K. G. Schnitzler, P. Wetzel, and J. Jungclaus (2007), Will the tropical land biosphere dominate the climate-carbon cycle feedback during the twenty-first century?, *Clim. Dyn.*, *29*, 565–574, doi:10.1007/s00382-007-0247-8.

Robock, A. (2000), Volcanic eruptions and climate, *Rev. Geophys.*, *38*, 191–219.

Schleussner, C. F., and G. Feulner (2013), A volcanically triggered regime shift in the subpolar North Atlantic Ocean as a possible origin of the Little Ice Age, *Clim. Past*, *9*, 1321–1330, doi:10.5194/cp-9-1321-2013.

Schmidt, G. A., et al. (2006), Present day atmospheric simulations using GISS Model E: Comparison to in-situ, satellite and reanalysis data, *J. Clim.*, *19*, 153–192.

Schmidt, G. A., et al. (2011), Climate forcing reconstructions for use in PMIP simulations of the last millennium (v1.0), *Geosci. Model Dev.*, *4*, 33–45, doi:10.5194/gmd-4-33-2011.

Schneider, D. P., C. M. Ammann, B. L. Otto-Bliesner, and D. S. Kaufman (2009), Climate response to large, high-latitude and low-latitude volcanic eruptions in the Community Climate System Model, *J. Geophys. Res.*, *114*, D15101, doi:10.1029/2008JD011222.

Shindell, D. T., G. A. Schmidt, R. L. Miller, and M. E. Mann (2003), Volcanic and solar forcing of climate change during the preindustrial era, *J. Clim.*, *16*, 4094–4107.

Steinhilber, F., J. Beer, and C. Frohlich (2009), Total solar irradiance during the Holocene, *Geophys. Res. Lett.*, *36*, L19704, doi:10.1029/2009GL040142.

Timmreck, C., S. J. Lorenz, T. J. Crowley, S. Kinne, T. J. Raddatz, M. A. Thomas, and J. H. Jungclaus (2009), Limited temperature response to the very large AD 1258 volcanic eruption, *Geophys. Res. Lett.*, *36*, L21708, doi:10.1029/2009GL040083.

Timmreck, C., H.-F. Graf, S. J. Lorenz, U. Niemeier, D. Zanchettin, D. Matei, J. H. Jungclaus, and T. J. Crowley (2010), Aerosol size confines climate response to volcanic super-eruptions, *Geophys. Res. Lett.*, *37*, L24705, doi:10.1029/2010GL045464.

Toohey, M., K. Kruger, U. Niemeier, and C. Timmreck (2011), The influence of eruption season on the global aerosol evolution and radiative impact of tropical volcanic eruptions, *Atmos. Chem. Phys.*, *11*, 12,351–12,367, doi:10.5194/acp-11-12351-2011.

Vieira, L. E. A., and S. Solanki (2010), Evolution of the solar magnetic flux on time scales of years to millenia, *Astron. Astrophys.*, *509*, doi:10.1051/0004-6361/200913276.

Wang, Y. M., J. L. Lean, and N. R. Sheeley Jr. (2005), Modeling the Sun's magnetic field and irradiance since 1713, *Astrophys. J.*, *625*, 522–538.

Watanabe, S., et al. (2010), MIROC-ESM 2010: Model description and basic results of CMIP5-20c3m experiments, *Geosci. Model Devel.*, *4*, 845–872, doi:10.5194/gmd-4-845-2011.

Wu, T., et al. (2013), Global carbon budgets simulated by the Beijing Climate Center Climate System Model for the last century, *J. Geophys. Res. Atmos.*, *118*, 4326–4347, doi:10.1002/jgrd.50320.

Zanchettin, D., O. Bothe, H. F. Graf, S. J. Lorenz, J. Luterbacher, C. Timmreck, and J. H. Jungclaus (2013), Background conditions influence the decadal climate response to strong volcanic eruptions, *J. Geophys. Atmos.*, *118*, 4090–4106, doi:10.1002/jgrd.50299.

Zhong, Y., G. H. Miller, B. Otto-Bliesner, M. Holland, D. Bailey, D. Schneider, and A. Geirsdottir (2010), Centennial-scale climate change from decadally-paced explosive volcanism: A coupled sea ice-ocean mechanism, *Clim. Dyn.*, *37*, 1–15, doi:10.1007/s00382-010-0967-z.